ADVANCED ENERGY MATERIALS
www.advenergymat.de

Toward More Efficient Organic Solar Cells: A Detailed Study of Loss Pathway and Its Impact on Overall Device Performance in Low-Offset Organic Solar Cells

Bowen Sun, Nurlan Tokmoldin, Obaid Alqahtani, Acacia Patterson, Catherine S. P. De Castro, Drew B. Riley, Manasi Pranav, Ardalan Armin, Frédéric Laquai, Brian A. Collins, Dieter Neher, and Safa Shoaee**

Low-offset organic solar cell systems have attracted great interest since nonfullerene acceptors came into the picture. While numerous studies have focused on the charge generation process in these low-offset systems, only a few studies have focused on the details of each loss channel in the charge generation process and their impact on the overall device performance. Here, several nonfullerene acceptors are blended with the same polymer donor to form a series of low-offset organic solar cell systems where significant variation in device performance is observed. Through detailed analyses of loss pathways, it is found that: i) the donor:acceptor interfaces of PM6:Y6 and PM6:TPT10 are close to the optimum energetic condition, ii) energetics at the donor:acceptor interface are the most important factor to the overall device performance, iii) exciton dissociation yield can be field-dependent owing to the sufficiently small energetic offset at the donor:acceptor interface, and iv) the change in substituents in the terminal group of Y-series acceptors in this work mainly affects energetics at the donor:acceptor interface instead of the interface density in the active layer. In general, this work presents a path toward more efficient organic solar cells.

1. Introduction

Thanks to the development of nonfullerene acceptors (NFAs), the organic solar cell (OSC) field is currently enjoying a revitalization, with power conversion efficiencies now approaching 20%.[1–3] Presently, OSC-based NFAs match their inorganic competitors in terms of current production (internal quantum efficiency) owing to their large and complementary absorption, but lag behind with regards to their fill factor (FF) and open-circuit voltage (V_{OC}).[4]

Interestingly, NFA-based solar cells seem to require a smaller driving force for charge generation to work efficiently and simultaneously benefit from a smaller open-circuit voltage loss. In this regard, PM6:Y6 has spurred significant fundamental interest for the possibility of an efficient device with a small energy offset. While initial reports on different NFA systems suggest that efficient charge generation is achievable with a small offset,[5–8] other in-depth characterization studies of energy levels suggest

B. Sun, N. Tokmoldin, S. Shoaee
Optoelectronics of Disordered Semiconductors
Institute of Physics and Astronomy
University of Potsdam
Karl-Liebknecht-Str. 24–25, 14476 Potsdam-Golm, Germany
E-mail: sun@uni-potsdam.de; shoai@uni-potsdam.de

B. Sun, M. Pranav, D. Neher
Soft Matter Physics and Optoelectronics
Institute of Physics and Astronomy
University of Potsdam
Karl-Liebknecht-Str. 24-25, 14476 Potsdam-Golm, Germany

The ORCID identification number(s) for the author(s) of this article can be found under https://doi.org/10.1002/aenm.202300980

DOI: 10.1002/aenm.202300980

O. Alqahtani, A. Patterson, B. A. Collins
Department of Physics and Astronomy
Washington State University
100 Dairy Road, Pullman, WA 99164, USA

O. Alqahtani
Department of Physics
Prince Sattam bin Abdulaziz University
Alkharj 11942, Kingdom of Saudi Arabia

C. S. P. De Castro, F. Laquai
KAUST Solar Center (KSC)
Physical Sciences and Engineering Division (PSE)
King Abdullah University of Science and Technology (KAUST)
Thuwal 23955-6900, Kingdom of Saudi Arabia

D. B. Riley, A. Armin
Sustainable Advanced Materials (Sêr SAM)
Department of Physics
Swansea University
Singleton Park, Swansea SA2 8PP, UK

that a minimum ionization potential offset of 0.3–0.5 eV is required to ensure efficient charge transfer.[9–11]

With decreasing the highest occupied molecular orbital (HOMO) offset, another observation is that the decreased energy offset between singlet excitons (S_1) and the charge transfer (CT) state of the acceptor (ΔE_{S_1-CT}) leads to reverse transition from the CT state back to the singlet state (repopulation of singlet excitons). Indeed, the low ΔE_{S_1-CT} feature and consequently S_1 reformation in low HOMO-offset systems can lead to interesting and important behaviors in these systems. For this reason, it was observed that the lowest nonradiative voltage losses (ΔV_{nr}) in such low-offset systems are defined by the photoluminescence yield of the acceptor.[12] However, recent work from Neher and co-workers shows that the reduction in ΔV_{nr} due to S_1 repopulation cannot be simply translated into an overall benefit to the V_{OC}.[13] On the other hand, the S_1 reformation feature changes the recombination picture, which can now occur via two channels – CT decay and S_1 decay. Recent work has shown that in PM6:Y6, while the S_1 emission dominates photoluminescence (PL) and electroluminescence (EL), around 99% of the recombination still occurs via the nonradiative CT channel.[14] However, in other systems with even smaller HOMO offset compared to that of PM6:Y6, the loss from the S_1 decay channel may be considerable.

In terms of the charge generation yield (CGY), it has been proposed in previous works that the relation between ΔE_{S_1-CT} and CGY can be well described by a model based on the Boltzmann stationary-state equilibrium between the CT and S_1 states when ΔE_{S_1-CT} is sufficiently small.[15] Thus, while the minimal energy offset inhibits the rate of charge transfer at the interface, a long exciton lifetime has been suggested to be a key to achieving high generation efficiencies in low ΔE_{S_1-CT} systems.[15,16] However, it has also been observed that other parameters such as the energetic offset between the CT and charge separation (CS) states, the CT decay rate (k_f), and morphology can play an important role in the relation between ΔE_{S_1-CT} and CGY.[17,18] In addition, it was also reported that the low ΔE_{S_1-CT} values influence the CT dissociation rate by affecting the energetic offset between the CT and CS states.[19]

Given these complex interplays, the question that arises is whether efficient organic solar cells could be obtained by simply reducing ΔE_{S_1-CT}. More specifically, how does the reduction of ΔE_{S_1-CT} affect the overall performance of an organic solar cell. While a considerable amount of work has focused on the effect of reduced ΔE_{S_1-CT} on V_{OC} and on charge generation, limited work has researched the effect of reduced ΔE_{S_1-CT} on charge recombination and fill factor and the overall device performance.[20,21]

In this work, a set of nonfullerene acceptors were judiciously selected and blended with the same polymer donor (PM6) and compared with the reference system PM6:Y6 to study the effect of reduced ΔE_{S_1-CT} on the overall performance. The systems in this work present a series of low ΔE_{S_1-CT} values with a wide range of device performances. Various steady-state and transient measurements were performed for a detailed study of charge generation, recombination, and V_{OC} losses. An insightful understanding of the role of ΔE_{S_1-CT} in the overall device performance in small ΔE_{S_1-CT} region is given. For the systems studied herein, we demonstrate that PM6:Y6 and PM6:TPT10 are close to the optimum energetic conditions with respect to their power conversion efficiency (PCE). In the systems where ΔE_{S_1-CT} values are further reduced, significant reduction in the short-circuit current (J_{SC}) and FF were observed concurrently with a limited benefit in V_{OC}, although ΔV_{nr} was significantly reduced. It was found that at J_{SC}, the losses mainly originated from inefficient exciton dissociation yield, while the losses via the CT states became more pronounced as the applied voltage reached V_{OC}.

Interestingly, the charge generation process was observed to be field-dependent in systems with sufficiently small ΔE_{S_1-CT} values. With further investigation, our data indicated that this field dependence came from field-dependent exciton dissociation at the donor:acceptor interface instead of from the CT states, presenting a different picture from that described by the Onsager–Braun model explaining a field-dependent charge generation in organic solar cells. Furthermore, the bimolecular recombination rate (k_2) increased as ΔE_{S_1-CT} was reduced. The field-dependent charge generation together with the increased k_2 leads to the inferior FF and the overall device performance in PM6:Y5 and PM6:o-IDTBR.

2. Results and Discussion

To study the relation between ΔE_{S_1-CT} and the device performance, three small NFA molecules are chosen as the acceptors (o-IDTBR, Y5, and TPT10) and PM6 is used as the donor. These three PM6:NFA systems are then compared with the "standardized" PM6:Y6 in terms of their device performances as well as detailed charge generation and recombination mechanisms and dynamics. The chemical structures of the three NFA molecules are given in **Figure 1**a, the full chemical names and device structures can be found in the Supporting Information. Compared to PM6:Y6, the three organic heterojunctions in this work have considerable smaller HOMO offsets, indicating smaller ΔE_{S_1-CT} values.

For the studied systems, while the HOMO offsets are only slightly different, significantly different device performances (in J_{SC}, FF, and V_{OC}) were observed. Figure 1d shows the currents–voltages (*JV*s) of the studied systems (detailed *JV* parameters are given in the Supporting Information), where the increase in V_{OC} comes at the cost of the reduction in J_{SC}. Among the studied systems, PM6:TPT10 has the largest J_{SC} (24.4 mA cm^{-2}) and lowest V_{OC} (0.91 V), while the behavior is vice versa for PM6:o-IDTBR (J_{SC} of 7.8 mA cm^{-2}, V_{OC} of 1.15 V). The photovoltaic bandgap of each system is obtained by the first derivative of photovoltaic external quantum efficiency (EQE_{PV}) spectra (Figure S1, Supporting Information). The low J_{SC} in PM6:o-IDTBR can be partly explained by its large photovoltaic bandgap (1.69 eV) compared to the other studied systems.

However, this is not the whole picture. As is shown in Figure 1d, the major difference in the EQE_{PV} spectra is in its amplitude rather than the absorption spectrum. In the following subsection, the ΔE_{S_1-CT} values of each system are first characterized and compared. Thereafter, detailed analyses on the charge generation and recombination are performed to elucidate the underlying origin of the device performance in these systems and give a unified understanding on the role of ΔE_{S_1-CT}.

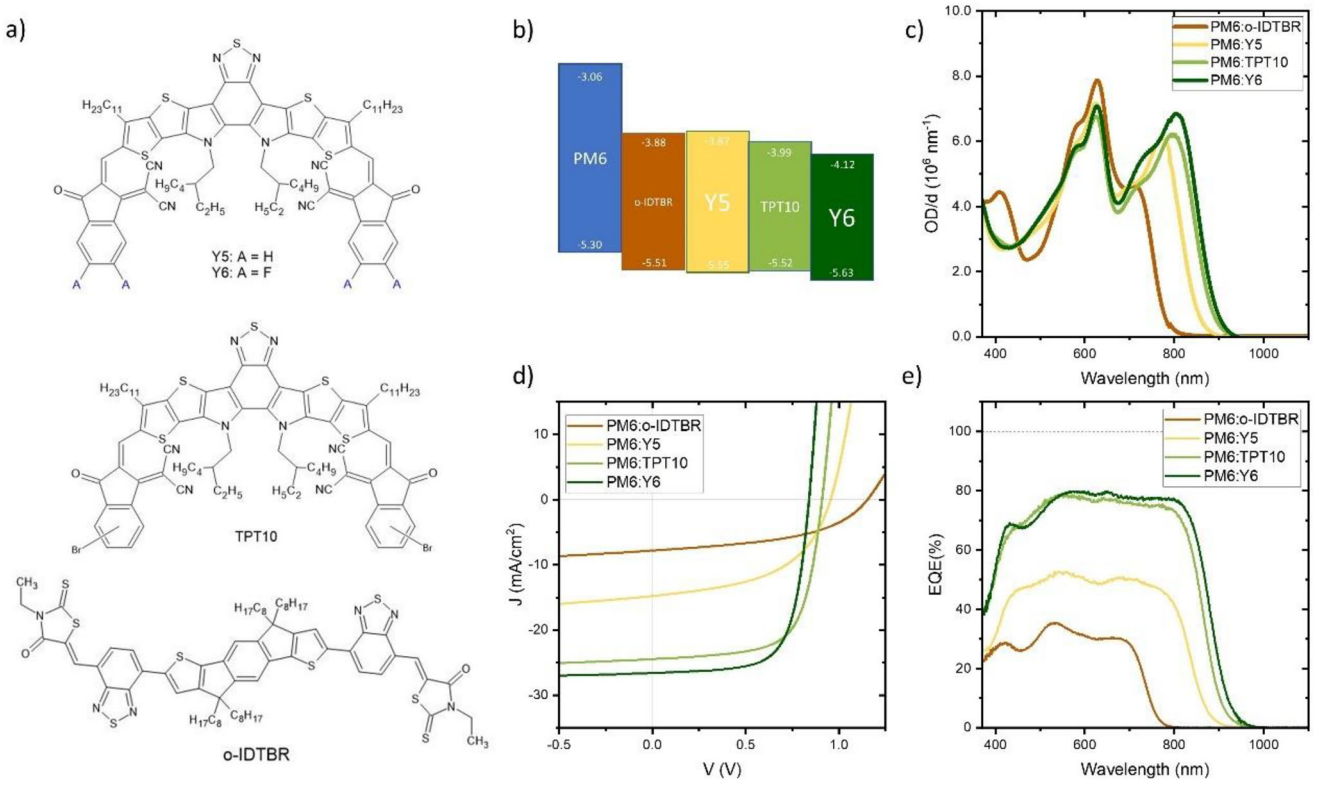

Figure 1. a) Chemical structures, b) energy levels of polymer donor and nonfullerene acceptors reported from previous work,[9,22–26] c) thickness-normalized optical densities, d) current–voltage (*JV*) characteristics, and e) external quantum efficiencies (EQEs) of the blends and materials used in this work.

2.1. Evaluation of Low ΔE_{S_1-CT} Offsets

In evaluating ΔE_{S_1-CT} by determining the HOMO–HOMO energetic offset, we are faced with two challenges: 1) difficulty in determining the HOMO values in the blend[27,28] and 2) lack of information on binding energies for the singlet exciton and CT states.[29–31] To overcome these issues, in particular account of the binding energies, and to study the energetics of the excited species in a working device, we consider using the energy difference between the CT state and the exciton, ΔE_{S_1-CT}, instead of HOMO–HOMO offset. To this end, we performed temperature-dependent electroluminescence quantum yield (T-ELQY) measurements on working devices. In a system where the HOMO–HOMO offset is estimated to be sufficiently small, the EL spectrum is almost entirely composed of the 0–0 transition of the small bandgap NFA singlet exciton (see Figure S2 in the Supporting Information).[14] In all three systems studied herein, the PL and EL of the blends resemble the PL of the neat acceptors (see Figure S2 in the Supporting Information for the comparison of the EL spectra of the blends and the PL spectra of the corresponding neat NFAs) pointing to the presence of the S_1 states and negligible CT contributions in the EL spectra, which is consistent with the energetics of the donor and acceptors.

In a T-ELQY measurement, when fixing the injection current, the quantity of reformed S_1 states is essentially the result of the rate competition between the CT decay and net S_1 repopulation rate from CT. While the rate constant of the CT decay is described by a constant k_f, the rate constant of S_1 reformation from CT can be described by an exponential expression $k_{ref} = k^*_{ref,0} \times \exp(-\frac{\Delta E_{S_1-CT}}{k_B T})$, where $k^*_{ref,0}$ corresponds to the net CT–S_1 reformation rate k_{ref} at infinite temperature.[14,32,33] In this regard, in the studied systems where the EL spectra are almost fully represented by exciton emission, the ELQY values are proportional to the quantity of reformed excitons in the charge injection process

$$\text{ELQY} \propto \frac{\#\text{exciton}}{\#\text{injected charge}} = \frac{k_{ref}(T)}{k_{ref}(T) + k_f} = \left[1 + \frac{k_f}{k_{ref}(T)}\right]^{-1} \quad (1)$$

Using the ELQY values, the normalized ELQY*(T) given by $\text{ELQY}^*(T) = \frac{\text{ELQY}(T)}{\text{ELQY}(T_{max})}$ is plotted against $1/k_B T$ and fitted with the physical model (Equation (1)), from which ΔE_{S_1-CT} is obtained. The data are shown in **Figure 2**a, where a clear trend of the ΔE_{S_1-CT} offset in the four involved systems is observed, varying from ≈25 (for PM6:o-IDTBR) to ≈114 meV (for PM6:Y6). The trend in ΔE_{S_1-CT} offsets agrees well with the EQE amplitudes (Figure 2b), where the smallest EQE corresponds to the smallest ΔE_{S_1-CT} offset. As the ΔE_{S_1-CT} offset increases, the EQE_{max} first increases accordingly, then saturates at ≈80%.

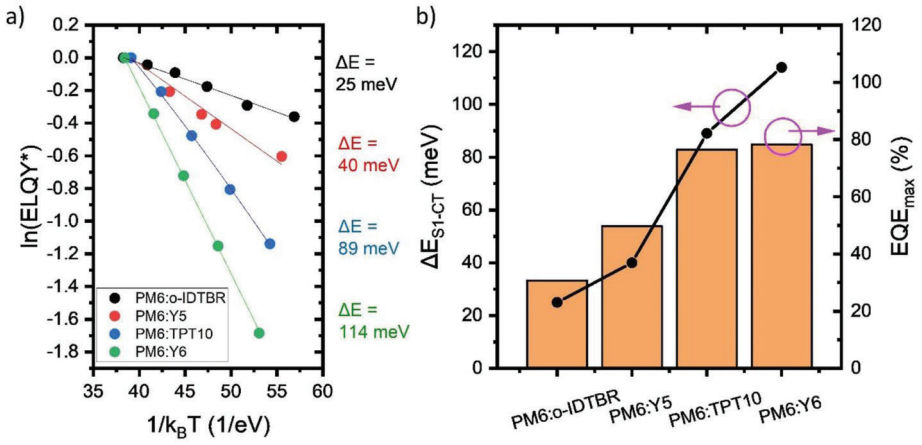

Figure 2. a) Temperature-dependent ELQY of the devices, the temperature-dependent ELQY values of PM6:Y6 are taken from a previous paper from our group,[14] and refitted with Equation (1). b) The fitted ΔE_{S_1-CT} values and EQE amplitude of each system.

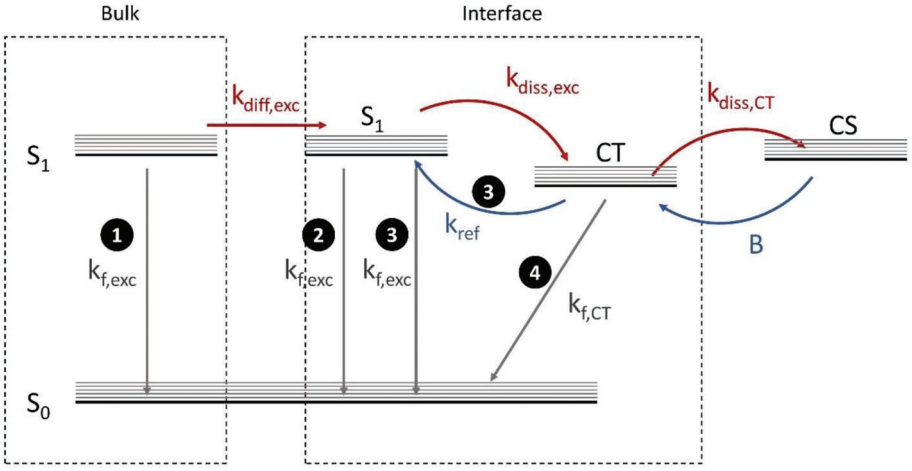

Figure 3. Energy diagram describing the generation and decay of S_1 and CT states as well as the interplays between each energy state in low-offset OSCs. $k_{f,exc}$, $k_{diff,exc}$, and $k_{diss,exc}$ are the rate constants of the decay, diffusion, and dissociation of excitons, respectively. $k_{f,CT}$ and $k_{diss,CT}$ are the rate constants of CT decay and CT dissociation, respectively. k_{ref} is the reformation rate constant, and B the rate of encounter of free carriers. The singlet excitons generated in the bulk diffuse to the donor:acceptor interface and dissociate to form CT states, and subsequently form free charges (CS) via CT dissociation. The CT and S_1 states can be repopulated upon the encounter of free charges and CT–S_1 reformation, respectively. Losses can occur through four channels: 1) via S_1 decay during the exciton diffusion in the bulk, 2) via S_1 decay during S_1 dissociation at the donor:acceptor interface, 3) via the decay of reformed S_1 from CT states, and 4) via CT decay.

2.2. Loss Channels in Low-Offset OSCs

For a deeper understanding of the losses in EQE and photocurrent in the studied systems, charge generation and recombination processes, as well as the interplays between each energy state must be considered (depicted in **Figure 3**). Light absorption by the bulk heterojunction (BHJ) materials generates excitons that diffuse to the donor:acceptor interfaces, where they dissociate into CT states which subsequently form CS states via CT dissociation. Upon the encounter of free charges, CT states are reformed and recombine directly to the ground state thereafter (known as bimolecular recombination). In low-offset OSC systems, the S_1 states can be rather efficiently repopulated via the CT state. The loss mechanism can be described by four channels: 1) exciton loss in the domain during exciton diffusion,[17,34] 2) decay of excitons at the donor:acceptor interface (energy driven),[34] 3) decay of reformed excitons from the CT states,[13,18] and 4) decay of the CT states. Channel 1 describes the competition between the domain size and exciton diffusion length, while channel 2 entails the details of the S_1 dissociation rate and exciton lifetime. On the other hand, channel 3 gives information on the competition between exciton reformation and CT decay, and channel 4 includes the rate competition between net CT dissociation, net CT reformation, and CT decay. In the following subsection, the losses from each channel are studied in detail.

2.3. Loss Analysis for J_{SC}

2.3.1. Losses via S_1 and CT States

Photoluminescence measurements can be used to probe exciton dissociation. The extent of exciton emission quenching of the

Table 1. The exciton diffusion length ($L_{D,acceptor}$) of the acceptors measured on neat acceptor films, as well as the characteristic length (L_C), exciton diffusion efficiency ($\eta_{exc,diff}$), and PL quenching (PL_{quen}) of each blend.

	$L_{D,acceptor}$ [nm]	L_C [nm]	Domain purity [N]	$\eta_{exc,diff}$	PL_{quen}
PM6:o-IDTBR	10	60	0.58	0.58	0.32
PM6:Y5	17	85	1	0.67	0.66
PM6:TPT10	17	110	0.7	0.58	0.94

blend film relative to the corresponding neat film can be a useful assay of exciton splitting, assigned to the charge transfer from the exciton to the formation of CT states. Herein, photoluminescence quantum yield (PLQY) and PL quenching measurements are performed to study the loss via the S_1 decay. For OSC systems with a large HOMO offset, when the blend is illuminated, the PL spectral characteristic is usually understood as a combination of exciton and CT decay. However, as is discussed in Section 2.1 in the discussion part, as ΔE_{S_1-CT} becomes sufficiently low, the CT states can more efficiently repopulate the S_1 state, and hence the PL spectrum is dominated by exciton contribution due to the much higher emissivity of the excitons compared to the CT states. With the PL emission in the studied systems being almost fully contributed by exciton emission (shown in Figure S2 in the Supporting Information), the PL quenching (PL_{quen}), which is calculated via Equation (2), represents the fraction of generated excitons that ultimately decay via nonradiative channels (e.g., CT and triplets). In large offset systems these are typically from the initially photogenerated excitons which do not dissociate to form a CT state, while in low offset systems, in addition to the photogenerated excitons, there is an additional contribution from reformed excitons via the CT state. The PL_{quen} values are tabulated in **Table 1** (The PLQY values of the blends and neat acceptors can be found in Table S2). As anticipated, exciton quenching becomes less and less efficient with decreasing offset.

$$PL_{quen} = 1 - \frac{PLQY_{Blend}}{PLQY_A} = \frac{\#\text{ quenched exciton}}{\#\text{ generated exciton}} \quad (2)$$

where $PLQY_{Blend}$ and $PLQY_A$ are the photoluminescence quantum yields of the donor:acceptor blend and neat acceptor, respectively.

Meanwhile, with the knowledge of optical constants (real refractive index n and extinction coefficient K) of each blend, the maximum photocurrent ($J_{ph,max}$) can be calculated for each studied system in terms of the optical transfer matrix,[35] under the assumption that all generated excitons are converted into free charges upon light excitation (see Note S2 in the Supporting Information for details). This serves as the upper limit of the photocurrent that the device could theoretically reach, limited by the absorption of the active layer. The ratio of J_{SC} and $J_{ph,max}$ evaluates the fraction of photogenerated excitons that are converted to free charges at the J_{SC} condition. A comparison of $J_{SC}/J_{ph,max}$ and PL_{quen} (at open-circuit voltage) for each system then evaluates the fraction of quenched excitons that results in free charges. As is presented in **Figure 4**c, the close agreement between $J_{SC}/J_{ph,max}$ and PL_{quen} values observed for all systems indicates the main loss

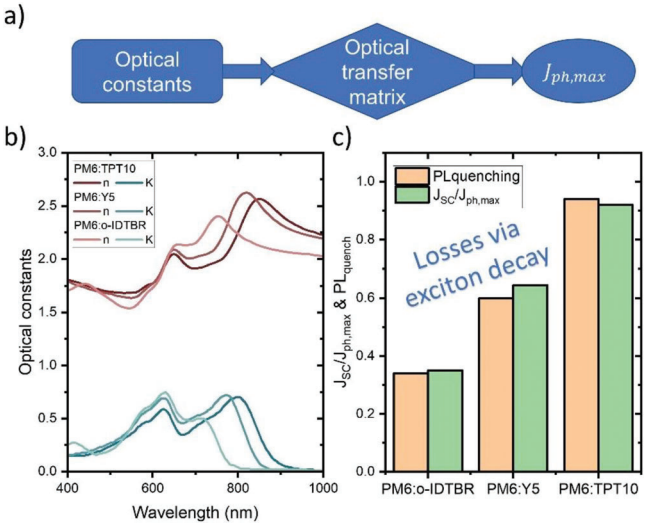

Figure 4. a) Calculation of maximum photocurrent ($J_{ph,max}$) in terms of the optical transfer matrix. b) The optical constants of each blend. c) Comparison of $J_{SC}/J_{ph,max}$ and PL quenching (at V_{OC}) of each system.

channel is the decay of S_1 (loss channels 1–3) rather than the CT state (loss channel 4).

2.3.2. Exciton Decay in the Bulk during Exciton Diffusion

While Figure 4c manifests the dominance of decay via S_1, we now delve deeper to decouple thermodynamics from kinetics of exciton diffusion in the bulk and charge transfer at the donor:acceptor interface. To address the exciton losses during the exciton diffusion process, a combination of characterizations of morphology, exciton lifetime, and diffusion length is conducted. Resonant soft X-ray scattering (R-SOXS) is a powerful technique to characterize the nanometer scale morphology and provide information of average domain size and domain purity in the active layer of organic solar cells.[36] Through the R-SOXS measurements, it was found that PM6:o-IDTBR has the smallest domain characteristic length (L_C), 60 nm, then PM6:Y5 (85 nm), and then PM6:TPT10 (110 nm). Given that the volume ratio of the donor and acceptor is close to 1 in our studied systems, the domain size in all studied systems is estimated to be half of their corresponding characteristic lengths.

The exciton diffusion lengths (L_D) and lifetimes (τ_{exc}) of the acceptors are measured by performing quasi-steady-state pulsed-PLQY measurements and time-resolved photoluminescence (TRPL) measurements on neat acceptor films, respectively (for TRPL measurement, the neat acceptor was diluted with polystyrene (PS), more details can be seen in the Experimental Section in the Supporting Information). The L_D of o-IDTBR was determined to be smallest among the three studied acceptors (≈10 nm), while those of Y5 and TPT10 were found to be much larger than that of o-IDTBR, with a similar value of ≈17 nm. The result of L_D is consistent with the τ_{exc} values obtained from TRPL, being 263, 1280, and 1071 ps for o-IDTBR, Y5, and TPT10, respectively. With the domain size and the exciton diffusion lengths, and assuming that the observed domains are 100% pure, the exciton diffusion efficiency ($\eta_{exc,diff}$,

representing the probability that an exciton reaches the interface) in each blend can be calculated with Equation (3)

$$\eta_{exc,diff} = \frac{2L_D}{\frac{1}{2}L_C} \tanh\left(\frac{\frac{1}{2}L_C}{2L_D}\right) \quad (3)$$

For all studied systems, the $\eta_{exc,diff}$ was found to be close to 0.6, showing no relation between $\eta_{exc,diff}$ and the observed trends in CGY and PL_{quen}. Notably, in PM6:TPT10, the calculated $\eta_{exc,diff}$ is much smaller than PL_{quen}. This discrepancy between $\eta_{exc,diff}$ and PL_{quen} can be explained by low domain purity in the studied systems. The relative domain purities in a set of binary organic heterojunctions can be estimated by R-SOXS, enabling a qualitative comparison in domain purities among the studied systems. The total scattering intensity (TSI) is related to Δn_{DA}, the contrast function of the donor and acceptor (see Figure S6 in the Supporting Information), by the relationship Domain purity $\propto \frac{\sqrt{TSI}}{|\Delta n_{DA}|}$. The domain purity was found to be the highest in PM6:Y5, then PM6:TPT10 (Table 1). The lowest domain purity was observed in PM6:o-IDTBR. As pointed out in numerous publications, less domain purity assists exciton dissociation by creating more donor:acceptor interfaces, leading to higher PL quenching.[37–41]

Another way of estimating the exciton diffusion efficiency relies on comparison between the saturated photocurrent $J_{ph,sat}$ measured with a high reverse bias and the theoretically calculated maximum photocurrent $J_{ph,max}$. Considering the domain purities, the ratio of $J_{ph,sat}$ over $J_{ph,max}$ represents the lower limit of exciton diffusion efficiency in the blends. Measuring the *JV* response of the three studied systems to obtain the ratio of photocurrent at each voltage $J_{ph}(V)$ and $J_{ph,max}$, it was found that the $J_{ph,sat}/J_{ph,max}$ values of both PM6:TPT10 and PM6:Y5 were close to 1 when measuring $J_{ph,sat}$ at −8 V (Figure S5, Supporting Information). Since the exciton diffusion process is independent of the applied field, this suggests that all generated excitons can successfully find the donor:acceptor interface in PM6:TPT10 and PM6:Y5. As for PM6:o-IDTBR at −8 V, $J_{ph,sat}/J_{ph,max}$ was found to be 0.73. In fact, considering the smallest domain size and lowest domain purity in PM6:o-IDTBR, it is considered that the actual exciton diffusion efficiency in PM6:o-IDTBR is also close to 1. In the following subsection, a calculation is performed to justify this point.

First, knowing the lower limit of exciton diffusion efficiency and exciton diffusion length, Equation (3) gives an estimation of the actual effective L_C in both PM6:TPT10 and PM6:Y5. We found a maximum value of ≈25 nm, significantly lower than the directly measured L_C from R-SOXS. According to the R-SOXS results, PM6:o-IDTBR has the smallest domain size and lowest domain purity, so the actual L_C in PM6:o-IDTBR should be even smaller than 25 nm. However, in the following subsection, we use L_C = 25 nm for the calculation to estimate the lowest exciton diffusion efficiency in PM6:o-IDTBR. With L_C = 25 nm and $L_{D,acceptor}$ = 10 nm (see Table 1) for PM6:o-IDTBR, the real exciton diffusion efficiency in PM6:o-IDTBR can be estimated to be at least 90%. Therefore, it could be concluded that in all studied systems, the excitons are able to find the donor:acceptor interface efficiently.

Notably, a relatively high FF of almost 70% is observed for PM6:TPT10 which is close to a Shockley-type charge extraction scenario.[42] This indicates that the charges can still be efficiently extracted in PM6:TPT10 despite its low domain purity, pointing to the formation of a descent intercrossing morphology between each impurity in the domains. Comparing the atomic force microscopy scans of the neat donor and acceptor as well as the blends, it was found that the fibrous feature from PM6 was well preserved in the films of donor:acceptor blends (Figure S7, Supporting Information). This is consistent with other studies with diluted PM6-based OSC systems, in that efficient charge transportation is ensured due to the high fibrous figure of the PM6 that connects each domain together.[43]

2.3.3. Exciton Decay at the Interface

For a better understanding of the mechanism behind the charge generation process, time delayed extraction field (TDCF) measurements were performed under very low fluences to study the field dependence of the charge generation yield (**Figure 5**c). It was found that the charge generation in systems with small ΔE_{S_1-CT} (PM6:o-IDTBR and PM6:Y5) is field-dependent, while in PM6:TPT10 and PM6:Y6, where ΔE_{S_1-CT} is relatively large, the charge generation is field-independent.[5] This further supports that the field-dependent current density between −2 and 0 V in the *JV* plot in PM6:o-IDTBR and PM6:Y5 (in Figure 1d) is due to actual charge generation processes instead of inefficient competition between charge extraction and recombination.

From the discussion in Sections 2.3.1 and 2.3.2, it is concluded that the differences in the EQE_{PV} amplitudes among the studied systems observed in Figure 1d mainly originate from the exciton losses at the donor–acceptor interface, giving an indication that the field dependence in charge generation originates from field-dependent exciton dissociation at the donor:acceptor interface instead of from field-dependent CT dissociation, as depicted by the Onsager–Braun model. This is further consolidated using comparisons between $J_{ph}/J_{ph,max}$ and PL quenching at three different applied voltages (V_{OC}, J_{SC}, and −2 V) shown in Figure 5a. It was observed that both $J_{ph}/J_{ph,max}$ and PL quenching increase while remaining close to each other when the applied bias changed from J_{SC} to −2 V. The similar but increasing PL quenching and $J_{ph}/J_{ph,max}$ values in PM6:Y5 and PM6:o-IDTBR evidence that in systems where ΔE_{S_1-CT} is sufficiently small: 1) at J_{SC}, exciton dissociation at the interface limits the photocurrent (through channels 2 and 3), and 2) the exciton dissociation yield at the donor:acceptor interface can be assisted with the application of an extraction bias. The field-dependent exciton dissociation yield, on the one hand, leads to inefficient CGY at J_{SC} and hence low EQE, and on the other hand leads to a reduction in FF.

At the V_{OC} condition where no charge extraction happens, $J_{ph}/J_{ph,max}$ becomes 0 while PL quenching remains relatively high. This indicates that at V_{OC}, the recombination current is mainly contributed by the CT decay (opposite to the situation at the J_{SC} condition).

As is highlighted in gray in Figure 5a, when applied voltage approaches V_{OC} from −2 V, recombination via the CT states (channel 4) is found to be more and more pronounced compared to the recombination via S_1. This is consistent with the observed discrepancy between the TDCF generation and *JV* data (Figure 5c, area highlighted in gray) showing that nongeminate

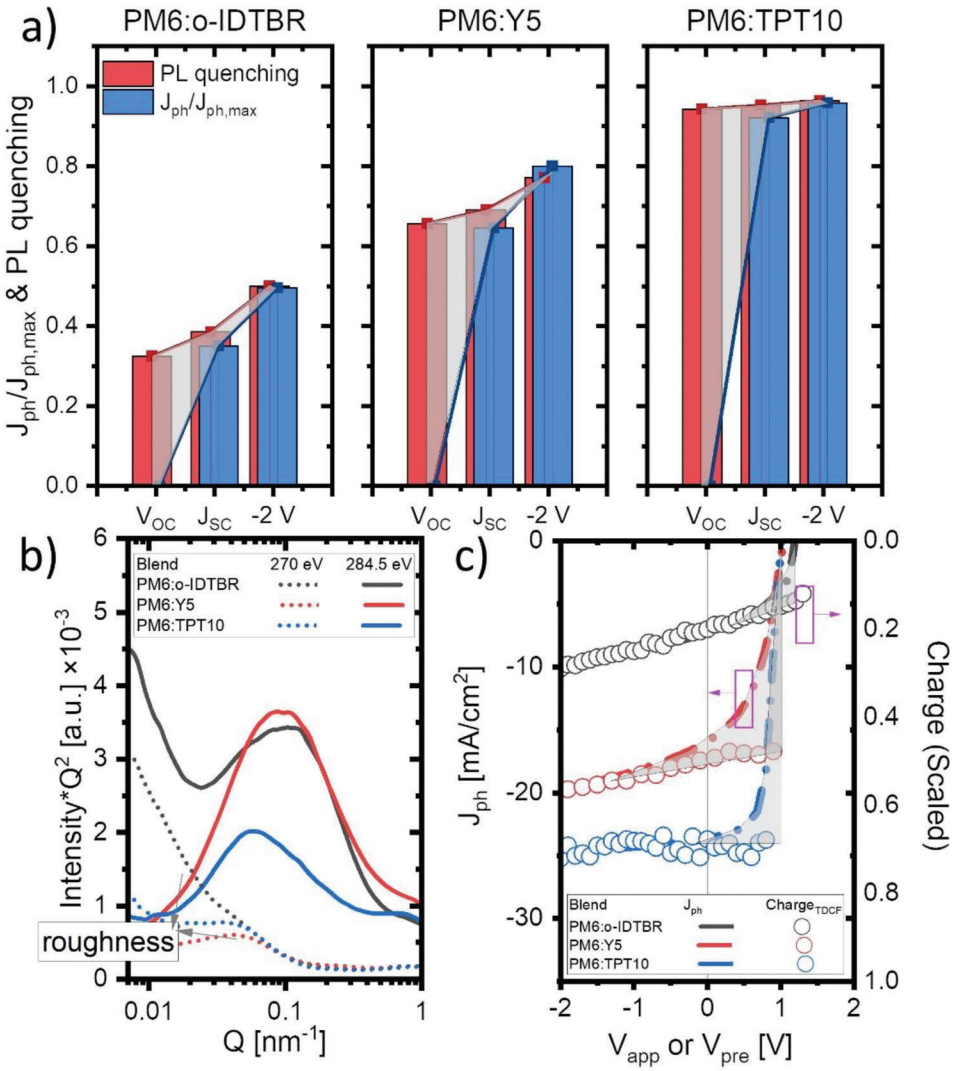

Figure 5. Comparison of the PL quenching and $J_{ph}/J_{ph,max}$ in a) V_{OC},J_{SC}, and reverse bias condition, b) R-SoXS profiles, and c) TDCF generation profile overlaid on J_{ph} $-V_{app}$ for PM6:o-IDTBR, PM6:Y5, and PM6:TPT10.

recombination due to an encounter of free charges becomes more significant as the applied bias approaches V_{OC} from reverse bias. The agreement in the gray highlighted areas in Figure 5a,c indicates, for all our studied systems, upon encountering of the free carriers, the decay is more likely to proceed via the CT states than by the CT–S_1 reformation and the consequent S_1 decay.

This is further evidenced by comparing the ELQY of the blends with the PLQY of the neat acceptors. Since the EL spectra of the donor:acceptor blend almost fully consists of the emission of acceptor excitons, ELQY presents the quantum yield of the blend to convert free charges into photons via exciton decay. Relating the PLQY of the neat acceptor (which is the probability that a formed acceptor exciton emits a photon) and the ELQY of the blend, the probability of recombination via exciton reformation and the subsequent exciton decay ($P_{ex,ref}$) upon the encounter of free carriers in each system (Figure 3, efficiency of channel 3) can be estimated by Equation (4). The ELQY of the blends and the PLQY of the neat acceptors, as well as $P_{ex,ref}$ in each studied system is summarized in Table S2 (Supporting Information). At near V_{OC}, the calculated $P_{ex,ref}$ in all studied systems is much smaller than 50%, with ≈3% for both PM6:TPT10 and PM6:o-IDTBR and 13% for PM6:Y5, which is consistent with the observation in Figure 5a,c that in all studied systems, recombination tends to proceed via channel 4 instead of channel 3 (depicted in Figure 3) upon the encounter of free carriers

$$P_{ex,ref} = \frac{ELQY_{blend}}{PLQY_A} \quad (4)$$

2.4. Charge Recombination

As shown in Figure 3, upon an encounter of free charges, exciton reformation is in competition with the CT decay process, and both contribute to bimolecular recombination. As derived in previous work, the effective bimolecular recombination rate k_{eff}

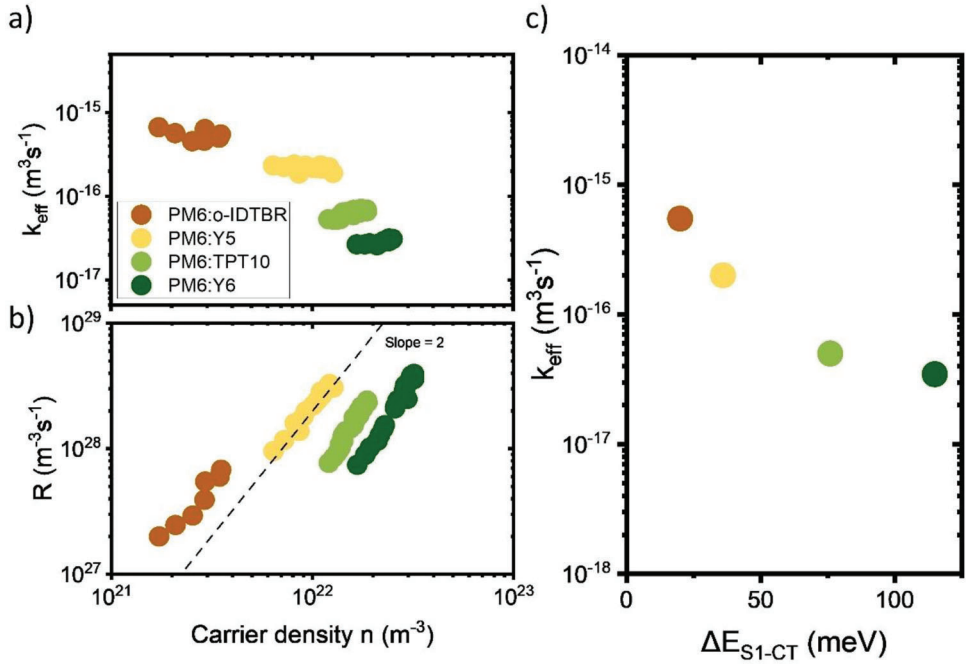

Figure 6. a) Effective bimolecular recombination rate coefficient k_{eff} and b) recombination rate R versus carrier density, and c) k_{eff} against ΔE_{S_1-CT} for PM6:o-IDTBR, PM6:Y5, PM6:TPT10, and PM6:Y6. The dashed line in (b) represents the slope of 2. The data for PM6:Y6 are taken from previous work from our group.[44]

given by $R_{CS} = k_{eff} n_{cs}^2$ can be obtained via Equation (5) for low-offset OSC systems[18]

$$k_{eff} = \left[\frac{1}{k_0} + \frac{1}{k_{CT} + k_S}\right]^{-1} \quad (5)$$

where k_0 is the charge encounter rate coefficient for free charge carriers, $k_{CT} = k_0 k_f / k_d$ is an effective bimolecular recombination coefficient via CT states, and $k_S = k_0 k_{bt}' / k_d$ is the corresponding effective bimolecular recombination coefficient for charge carriers to ultimately decay via excitons. The ratio between k_{CT} and k_S is given by k_f / k_{bt}'. k_f is the CT state recombination rate constant, and k_{bt}' is the back-transfer rate constant for CT states to recombine via excitons in the acceptor, which increases exponentially as ΔE_{S_1-CT} decreases. As Equation (5) indicates, when the CT decay rate constant (k_f) is much faster than k_{bt}', the S_1 reformation process is minor and does not have much effect on the overall recombination process. However, as k_{bt}' increases, the S_1 reformation starts to act as a loss channel and contributes to the recombination process. This means when ΔE_{S_1-CT} gets small enough, either the CT recombination itself is so fast and dominates the recombination rate, or the S_1 decay acts as another leakage channel to the overall recombination rate. Both of the above-described cases lead to a reduction in FF and hence are not favorable for the overall device performance.

In general, reduced ΔE_{S_1-CT} increases k_{eff}, and the significance of this effect depends on the rate competition between CT decay and S_1 reformation, and the subsequent S_1 decay. To study the effect of ΔE_{S_1-CT} on the bimolecular recombination rate k_{eff}, bias assisted charge extraction measurements were performed for each system that is studied here. This charge extraction method estimates the carrier density at various fluence at V_{OC} condition and calculates the effective bimolecular recombination rate via $G = R = k_{eff} n_{cs}^2$. As shown in **Figure 6**, it was found that the measured k_{eff} reduces by 1 order from 3×10^{-16} to 3×10^{-17} m^3 s^{-1} as ΔE_{S_1-CT} increases from 25 to 114 meV which is consistent with the result from Equation (5) and the discussion in the previous paragraph.

2.5. V_{OC} Losses in Low-Offset OSCs

It has been found in previous work that the ΔV_{nr} value gets significantly suppressed in systems with low ΔE_{S_1-CT}, and its lowest limit is defined by the PLQY of the pristine low-optical bandgap material of the blend.[12] In our study, ΔV_{nr} of each system was determined via $\Delta V_{nr} = k_B T \cdot \ln(\text{ELQY})$. The ELQY values in the systems with low ΔE_{S_1-CT}, PM6:o-IDTBR and PM6:Y5 (1.6×10^{-3} and 3.2×10^{-3}, respectively), were found to be much higher than those in systems with relatively high ΔE_{S_1-CT} (PM6:TPT10 and PM6:Y6, with values of 7.4×10^{-4} and 2.7×10^{-5}, respectively), leading to a very low ΔV_{nr} value of 0.16 eV – one of the lowest ΔV_{nr} values in organic solar cells. However, interestingly, when analyzing the overall V_{OC} losses using the difference between the photovoltaic bandgap of the system (E_g) and measured V_{OC},[45] it was found that the overall V_{OC} losses among the studied systems are very close (**Figure 7**, left panel).

To further investigate into the observed discrepancy between the trends in overall V_{OC} losses and ΔV_{nr} among the studied systems, the radiative voltage limit $V_{OC,rad}$ was evaluated for each system with Equation (6)[46] (more details about the determination of $V_{OC,rad}$ can be found in the Supporting Information). Getting

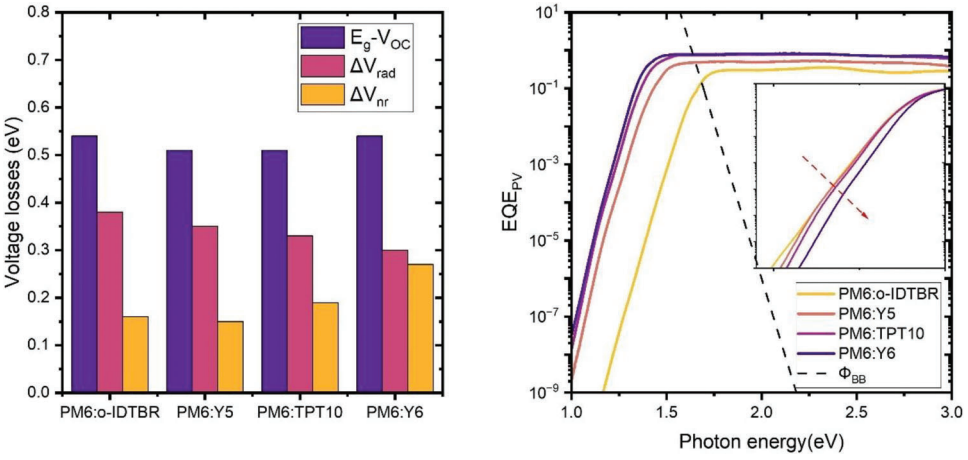

Figure 7. Left panel: the overall, radiative, and nonradiative voltage losses of PM6:o-IDTBR, PM6:Y5, PM6:TPT10, and PM6:Y6. The dashed dotted lines are guides to the eye. The data for PM6:Y6 are from previous work from our group.[14] Right panel: the extended EQE_{PV} spectra of PM6:o-IDTBR, PM6:Y5, PM6:TPT10, and PM6:Y6 spectra. Inset, zoomed-in and all the EQE_{PV} spectra are merged at the kink (where sub-bandgap starts) – in order to give a more intuitive comparison on the slope for each system.

the radiative voltage loss ΔV_{rad} via $\Delta V_{rad} = E_g - V_{OC,\,rad}$, and plotting ΔV_{rad} together with ΔV_{nr} for each system, an anticorrelation can be found between these two parameters (Figure 7, left panel). From PM6:o-IDTBR to PM6:Y6, while ΔE_{S_1-CT} increases, the increase in ΔV_{nr} and reduction in ΔV_{rad} compensate each other and lead to a constant overall V_{OC} loss

$$q \cdot V_{OC,\,rad} = k_B T \cdot \ln\left(\frac{J_R}{J^0_{rad}}\right) \tag{6}$$

where where J_R is the total recombination current, J^0_{rad} is the radiative dark saturation current density.

As shown in Figure 7 (left panel), there seems to be a relation between ΔE_{S_1-CT}, ΔV_{nr}, and ΔV_{rad}. This is reminiscent of the relation between the S_1 population and ΔE_{S_1-CT} which can affect both ΔV_{nr} and ΔV_{rad} due to the high emissivity of S_1 compared to the CT states.[13] However, in all systems studied here, the ΔE_{S_1-CT} is so small that the contributions of the CT state to the EQE_{PV} spectra are nearly negligible. This is evidenced from a) the EL measurements (which is related to EQE_{PV} via reciprocity) showing that the EL spectra are almost entirely contributed by S_1, and b) previous ultrasensitive EQE_{PV} measurements for PM6:Y6 where no observable CT contribution is presented.[5] This means that for all systems, J^0_{rad}, and with this $V_{OC,rad}$, is entirely determined by the properties of the singlet exciton and have no "functional" dependence on ΔE_{S_1-CT}. Instead, the difference in the ΔV_{rad} observed in our systems is found to be due to the subtle difference in the shapes of the tails in the EQE_{PV} spectra. For example, PM6:Y6 gives the sharpest tail while PM6:o-IDTBR has the "flattest" tail, as can be more intuitively found in the inset of Figure 7 on the right panel. This affects the calculated J^0_{rad} values when convoluting the EQE_{PV} spectra with the blackbody photon flux and thus the ΔV_{rad}. In other words, the increase of ΔV_{rad} when decreasing ΔE_{S_1-CT} comes from a broadening of the EQE_{PV} spectra rather from the S_1 repopulation process. The reason is suspected to be lying in the stiffness of the NFA and detailed blend morphology. Therefore, it is not evident that the observed dependence of ΔV_{rad} on ΔE_{S_1-CT} among the systems involved in this study can be generalizable, but it is worth studying this case for more systems in the future.

3. Conclusion

In conclusion, by performing detailed analyses of overall efficiency losses to a series of NFA-based low-offset systems, our work shows that both J_{SC} and FF are severely reduced as ΔE_{S_1-CT} becomes sufficiently small, yet the reduction in V_{OC} losses is limited, despite the significantly reduced ΔV_{nr}. In all systems studied herein, the losses in J_{SC} conditions were assigned to exciton dissociation at the donor:acceptor interface. The exciton loss at the donor:acceptor interface was found to be more significant in the systems with the smallest ΔE_{S_1-CT} value. Importantly, in the two systems with the lowest ΔE_{S_1-CT} values (PM6:o-IDTBR and PM6:Y5), exciton dissociation yield at the donor:acceptor interface was found to be field-dependent, which also leads to a further reduction in the FF. In the forward bias regime where bimolecular recombination becomes significant, recombination via the CT state was found to be increasingly pronounced as the applied bias approached V_{OC}. Thus, despite the presence of S_1 reformation and the consequent decay via S_1, recombination via CT state still serves as the prominent decay channel of the encountered free electrons and holes and severely affects FF, even in the system with very small ΔE_{S_1-CT}. In addition, consistent with previous theoretical work,[18] it was found that decreasing ΔE_{S_1-CT} is not beneficial for achieving low bimolecular recombination coefficients. We anticipate this is due to a stronger binding energy of the CT state (when it becomes closer to the S_1 state), reducing the probability of redissociation. In general, the results in our study support an inferior PCE obtained by simply reducing ΔE_{S_1-CT} from PM6:TPT10 and PM6:Y6. In addition, our work provides structure–function information by showing that upon a change of the halogen substituents in the terminal groups of Y5, TPT10, and Y6, the exciton diffusion in their binary heterojunctions with PM6 remain highly efficient, while the very different *JV*

performances among these three systems mainly rely on the energetics at the interface.

Supporting Information

Supporting Information is available from the Wiley Online Library or from the author.

Acknowledgements

The authors acknowledge funding from the Deutsche Forschungsgemeinschaft (DFG, German Research Foundation) through the project Fabulous (Project Number 450968074) and Extraordinaire (Project Number 460766640). The R-SOXS and morphology characterization were supported by the U.S. Department of Energy Early Career Research Program under Grant No. DE-SC0017923 and used resources of the Advanced Light Source, which is a DOE Office of Science User facility under Contract No. DE-AC02-05CH11231; also used the resources of the SST-1 beamline (Beamline 7-ID-1) of the National Synchrotron Light Source II, a U.S. Department of Energy (DOE) Office of Science User Facility operated for the DOE Office of Science by Brookhaven National Laboratory under Contract No. DESC0012704. This publication is based upon work supported by King Abdullah University of Science and Technology (KAUST) under Award No. ORFS-CRG7-2019-4025. The pulsed-PLQY measurement was supported by the Welsh Government's Sêr Cymru II Program through the European Regional Development Fund, Welsh European Funding Office, and Swansea University strategic initiative in Sustainable Advanced Materials. A.A. is a Sêr Cymru II Rising Star Fellow. D.B.R. acknowledges the support of the Natural Sciences and Engineering Research Council of Canada (NSERC) (Grant No. PGSD3-545694-2020).

Open access funding enabled and organized by Projekt DEAL.

Conflict of Interest

The authors declare no conflict of interest.

Data Availability Statement

The data that support the findings of this study are available from the corresponding author upon reasonable request.

Keywords

exciton reformation, field-dependent exciton dissociation, loss pathways, low-offset NFA organic solar cells, structure–function relationships

Received: April 1, 2023
Revised: April 27, 2023
Published online: May 17, 2023

[1] Y. Wei, Z. Chen, G. Lu, N. Yu, C. Li, J. Gao, X. Gu, X. Hao, G. Lu, Z. Tang, J. Zhang, Z. Wei, X. Zhang, H. Huang, *Adv. Mater.* **2022**, *34*, 2204718.

[2] L. Zhu, M. Zhang, J. Xu, C. Li, J. Yan, G. Zhou, W. Zhong, T. Hao, J. Song, X. Xue, Z. Zhou, R. Zeng, H. Zhu, C.-C. C. Chen, R. C. I. I. MacKenzie, Y. Zou, J. Nelson, Y. Zhang, Y. Sun, F. Liu, *Nat. Mater.* **2022**, *21*, 656.

[3] W. Gao, F. Qi, Z. Peng, F. R. Lin, K. Jiang, C. Zhong, W. Kaminsky, Z. Guan, C.-S. Lee, T. J. Marks, H. Ade, A. K.-Y. Jen, *Adv. Mater.* **2022**, *34*, 2202089.

[4] M. A. Green, E. D. Dunlop, J. Hohl-Ebinger, M. Yoshita, N. Kopidakis, X. Hao, *Prog. Photovoltaics* **2020**, *28*, 629.

[5] L. Perdigón-Toro, H. Zhang, A. Markina, J. Yuan, S. M. Hosseini, C. M. Wolff, G. Zuo, M. Stolterfoht, Y. Zou, F. Gao, D. Andrienko, S. Shoaee, D. Neher, *Adv. Mater.* **2020**, *32*, 1906763.

[6] S. Li, L. Zhan, C. Sun, H. Zhu, G. Zhou, W. Yang, M. Shi, C. Z. Li, J. Hou, Y. Li, H. Chen, *J. Am. Chem. Soc.* **2019**, *141*, 3073.

[7] R. Wang, J. Yuan, R. Wang, G. Han, T. Huang, W. Huang, J. Xue, H. C. Wang, C. Zhang, C. Zhu, P. Cheng, D. Meng, Y. Yi, K. H. Wei, Y. Zou, Y. Yang, *Adv. Mater.* **2019**, *31*, 1904215.

[8] Y. Zhong, M. Causa', G. J. Moore, P. Krauspe, B. Xiao, F. Günther, J. Kublitski, R. Shivhare, J. Benduhn, E. BarOr, S. Mukherjee, K. M. Yallum, J. Réhault, S. C. B. Mannsfeld, D. Neher, L. J. Richter, D. M. DeLongchamp, F. Ortmann, K. Vandewal, E. Zhou, N. Banerji, *Nat. Commun.* **2020**, *11*, 833.

[9] D. Neusser, B. Sun, W. L. Tan, L. Thomsen, T. Schultz, L. Perdigón-Toro, N. Koch, S. Shoaee, C. R. McNeill, D. Neher, S. Ludwigs, L. Perdigón Toro, N. Koch, S. Shoaee, C. R. McNeill, D. Neher, S. Ludwigs, *J. Mater. Chem.* **2022**, *10*, 11565.

[10] J. Bertrandie, J. Han, C. S. P. De Castro, E. Yengel, J. Gorenflot, T. Anthopoulos, F. Laquai, A. Sharma, D. Baran, *Adv. Mater.* **2022**, *34*, 2202575.

[11] S. Karuthedath, J. Gorenflot, Y. Firdaus, N. Chaturvedi, C. S. P. De Castro, G. T. Harrison, J. I. Khan, A. Markina, A. H. Balawi, T. A. Dela Peña, W. Liu, R. Z. Liang, A. Sharma, S. H. K. Paleti, W. Zhang, Y. Lin, E. Alarousu, D. H. Anjum, P. M. Beaujuge, S. De Wolf, I. McCulloch, T. D. Anthopoulos, D. Baran, D. Andrienko, F. Laquai, *Nat. Mater.* **2021**, *20*, 378.

[12] X.-K. K. Chen, D. Qian, Y. Wang, T. Kirchartz, W. Tress, H. Yao, J. Yuan, M. Hülsbeck, M. Zhang, Y. Zou, Y. Sun, Y. Li, J. Hou, O. Inganäs, V. Coropceanu, J.-L. L. Bredas, F. Gao, *Nat. Energy* **2021**, *6*, 799.

[13] T. Fritsch, J. Kurpiers, S. Roland, N. Tokmoldin, S. Shoaee, T. Ferron, B. A. Collins, S. Janietz, K. Vandewal, D. Neher, *Adv. Energy Mater.* **2022**, *12*, 2200641.

[14] L. Perdigón-Toro, L. Q. Phuong, S. Zeiske, K. Vandewal, A. Armin, S. Shoaee, D. Neher, *ACS Energy Lett.* **2021**, *6*, 557.

[15] A. Classen, C. L. Chochos, L. Lüer, V. G. Gregoriou, J. Wortmann, A. Osvet, K. Forberich, I. McCulloch, T. Heumüller, C. J. Brabec, *Nat. Energy* **2020**, *5*, 711.

[16] T. F. Hinrichsen, C. C. S. Chan, C. Ma, D. Paleček, A. Gillett, S. Chen, X. Zou, G. Zhang, H.-L. Yip, K. S. Wong, R. H. Friend, H. Yan, A. Rao, P. C. Y. Chow, *Nat. Commun.* **2020**, *11*, 5617.

[17] D. B. Riley, P. Meredith, A. Armin, O. J. Sandberg, *J. Phys. Chem. Lett.* **2022**, *13*, 4402.

[18] O. J. Sandberg, A. Armin, *J. Phys. Chem.* **2021**, *125*, 15590.

[19] M. Azzouzi, N. P. Gallop, F. Eisner, J. Yan, X. Zheng, H. Cha, Q. He, Z. Fei, M. Heeney, A. A. Bakulin, J. Nelson, *Energy Environ. Sci.* **2022**, *15*, 1256.

[20] X. Zhang, N. Yao, R. Wang, Y. Li, D. Zhang, G. Wu, J. Zhou, X. Li, H. Zhang, J. Zhang, Z. Wei, C. Zhang, H. Zhou, F. Zhang, Y. Zhang, *Nano Energy* **2020**, *75*, 105032.

[21] A. Karki, J. Vollbrecht, A. J. Gillett, P. Selter, J. Lee, Z. Peng, N. Schopp, A. L. Dixon, M. Schrock, V. Nádaždy, F. Schauer, H. Ade, B. F. Chmelka, G. C. Bazan, R. H. Friend, T. Q. Nguyen, *Adv. Energy Mater.* **2020**, *10*, 2001203.

[22] S. Chen, Y. Wang, L. Zhang, J. Zhao, Y. Chen, D. Zhu, H. Yao, G. Zhang, W. Ma, R. H. Friend, P. C. Y. Chow, F. Gao, H. Yan, *Adv. Mater.* **2018**, *30*, 1804215.

[23] R. Qin, D. Wang, G. Zhou, Z. P. Yu, S. Li, Y. Li, Z. X. Liu, H. Zhu, M. Shi, X. Lu, C. Z. Li, H. Chen, *J. Mater. Chem.* **2019**, *7*, 27632.

[24] Q. Fan, Q. An, Y. Lin, Y. Xia, Q. Li, M. Zhang, W. Su, W. Peng, C. Zhang, F. Liu, L. Hou, W. Zhu, D. Yu, M. Xiao, E. Moons, F. Zhang, T. D. Anthopoulos, O. Inganäs, E. Wang, *Energy Environ. Sci.* **2020**, *13*, 5017.

[25] J. Yuan, Y. Zhang, L. Zhou, C. Zhang, T. K. Lau, G. Zhang, X. Lu, H. L. Yip, S. K. So, S. Beaupré, M. Mainville, P. A. Johnson, M. Leclerc, H. Chen, H. Peng, Y. Li, Y. Zou, *Adv. Mater.* **2019**, *31*, 1807577.
[26] C. Sun, S. Qin, R. Wang, S. Chen, F. Pan, B. Qiu, Z. Shang, L. Meng, C. Zhang, M. Xiao, C. Yang, Y. Li, *J. Am. Chem. Soc.* **2020**, *142*, 1465.
[27] K. Bruchlos, D. Trefz, A. Hamidi-Sakr, M. Brinkmann, J. Heinze, A. Ruff, S. Ludwigs, *Electrochim. Acta* **2018**, *269*, 299.
[28] M. Schwarze, W. Tress, B. Beyer, F. Gao, R. Scholz, C. Poelking, K. Ortstein, A. A. Günther, D. Kasemann, D. Andrienko, K. Leo, *Science* **2016**, *352*, 1446.
[29] C. M. Cardona, W. Li, A. E. Kaifer, D. Stockdale, G. C. Bazan, *Adv. Mater.* **2011**, *23*, 2367.
[30] J. Sworakowski, J. Lipiński, K. Janus, *Org. Electron.* **2016**, *33*, 300.
[31] R. E. M. Willems, C. H. L. Weijtens, X. de Vries, R. Coehoorn, R. A. J. Janssen, *Adv. Energy Mater.* **2019**, *9*, 1803677.
[32] W. Li, S. Zeiske, O. J. Sandberg, D. B. Riley, P. Meredith, A. Armin, *Energy Environ. Sci.* **2021**, *14*, 6484.
[33] C. L. Braun, *J. Chem. Phys.* **1984**, *80*, 4157.
[34] A. Armin, W. Li, O. J. Sandberg, Z. Xiao, L. Ding, J. Nelson, D. Neher, K. Vandewal, S. Shoaee, T. Wang, H. Ade, T. Heumüller, C. Brabec, P. Meredith, *Adv. Energy Mater.* **2021**, *11*, 2003570.
[35] G. F. Burkhard, E. T. Hoke, M. D. McGehee, *Adv. Mater.* **2010**, *22*, 3293.
[36] B. A. Collins, E. Gann, *J. Polym. Sci.* **2022**, *60*, 1199.
[37] O. Alqahtani, M. Babics, J. Gorenflot, V. Savikhin, T. Ferron, A. H. Balawi, A. Paulke, Z. Kan, M. Pope, A. J. Clulow, J. Wolf, P. L. Burn, I. R. Gentle, D. Neher, M. F. Toney, F. Laquai, P. M. Beaujuge, B. A. Collins, *Adv. Energy Mater.* **2018**, *8*, 1702941.
[38] N. A. Ran, J. A. Love, M. C. Heiber, X. Jiao, M. P. Hughes, A. Karki, M. Wang, V. V. Brus, H. Wang, D. Neher, H. Ade, G. C. Bazan, T. Nguyen, *Adv. Energy Mater.* **2018**, *8*, 1701073.
[39] K. D. Rosenthal, M. P. Hughes, B. R. Luginbuhl, N. A. Ran, A. Karki, S. Ko, H. Hu, M. Wang, H. Ade, T. Nguyen, *Adv. Energy Mater.* **2019**, *9*, 1901077.
[40] B. A. Collins, Z. Li, J. R. Tumbleston, E. Gann, C. R. McNeill, H. Ade, *Adv. Energy Mater.* **2013**, *3*, 65.
[41] L. Ye, S. Li, X. Liu, S. Zhang, M. Ghasemi, Y. Xiong, J. Hou, H. Ade, *Joule* **2019**, *3*, 443.
[42] D. Neher, J. Kniepert, A. Elimelech, L. J. A. Koster, *Sci. Rep.* **2016**, *6*, 24861.
[43] N. Yao, J. Wang, Z. Chen, Q. Bian, Y. Xia, R. Zhang, J. Zhang, L. Qin, H. Zhu, Y. Zhang, F. Zhang, *J. Phys. Chem. Lett.* **2021**, *12*, 5039.
[44] S. M. Hosseini, N. Tokmoldin, Y. W. Lee, Y. Zou, H. Y. Woo, D. Neher, S. Shoaee, *Sol. RRL* **2020**, *4*, 2000498.
[45] Y. Wang, D. Qian, Y. Cui, H. Zhang, J. Hou, K. Vandewal, T. Kirchartz, F. Gao, *Adv. Energy Mater.* **2018**, *8*, 1801352.
[46] U. Rau, *Phys. Rev. B* **2007**, *76*, 085303.